International Space Planes and Hypersonic Systems and Technologies Conferences
6-9 March 2017, Xiamen, China
21st AIAA International Space Planes and Hypersonics Technologies Conference

10.2514/6.2017-2277

Development of zone flamelet model for scramjet combustor modeling

Wei Yao[1a,b] Xuejun Fan[2a,b*]

a. Key Laboratory of High Temperature Gas Dynamics, Institute of Mechanics, CAS, No.15 Beisihuanxi Road, Beijing 100190, China

b. School of Engineering Science, University of Chinese Academy of Science, Beijing 100049, China

To alleviate the huge computational cost in supersonic combustor modeling and to improve the accuracy of traditional unsteady flamelet model, a zone flamelet is proposed. The main idea of zone flamelet is to divide the whole turbulent combustion field into a finite number of control zones and the chemical status in each zone is represented by a single flamelet. With proper zone division, the scattering of variables over the mixture fraction space is in controllable small, thus the representative flamelet approaches the real scalar distribution. The flamelets exchange information through flux-conserved convection when across the zone boundary, thus the flamelet variables can be transport from upstream to downstream in a flow manner. Although one additional mixture fraction space is resolved, great computational cost is still saved because the zone division in physical space is much coarser than the flow simulation mesh. A simple historical statistics approach is proposed to estimate the representative temperature, in order to further alleviate the computational cost in solving the flamelet temperature equation usually with numerous sub-models for non-adiabatic terms, e.g. radiation and wall heat loss. The zone flamelet model is then applied to model a scramjet combustor operated at a flight Mach number of 6.5 and a fuel equivalence ratio of 0.8. The performance of zone flamelet model in highly non-equilibrium supersonic combustion is compared with the traditional PaSR model.

I. Introduction

Experimental measurement of scramjet combustors are difficult, due mainly to the severe thermal load for instruments and the drastic distortion of supersonic flow field by probing disturbance. Especially the time-variance and spatial inhomogeneity of high-Re (Reynolds number) supersonic combustion fields requires transient and three-dimensional information to understand the flow physics in supersonic combustors. Due to the incapability of physical sensors for supersonic combustor measurements, the measurement data are generally scare and can be generally classified as two types. The first type of measurement data is used to analyze the combustion characteristics, including those field information of pressure, temperature, velocity and species concentrations etc. The other type is used to evaluate the combustor performance, including those combustion efficiency, total pressure loss, internal friction drag, wall heat flux and net thrust etc. The second type of data are

[1] Associate Professor, Institute of Mechanics (CAS), weiyao@imech.ac.cn, AIAA member.

[2] Professor, Institute of Mechanics (CAS), xfan@imech.ac.cn, AIAA lifetime member.

slightly easier to obtain without the need of using intrusive instruments (at least not in the high-temperature core) while the measurement of the first type of data requires the using of non-intrusive optical techniques, such as CARS (Coherent Anti-Stokes Raman Scattering) [1, 2], PLIF (planar induced laser fluorescence) [3-5] and schlieren [4, 5] systems. However, the non-intrusive optical techniques still can only provide planar or zonal flowfield information, the three-dimensional flow structures as well as their evolution physics cannot be revealed solely by the measurements. From this point of view, high-fidelity numerical modeling is almost the only way to gain deep and comprehensive insights into the internal flow, mixing and combustion processes in scramjet combustors [6-8].

An intricate problem in modeling the full-scale supersonic combustors is the resolving of turbulence-chemistry interaction, which is complex in nature since multiple physical scales are involved and usually takes much more computational cost than the frozen flow modeling. To accurately resolving the unsteady flow, mixing and combustion processes as well as the related flow structures in supersonic combustors, LES (Large Eddy Simulation) or DNS (Direct Numerical Simulation) based high-resolution, and of course computationally expansive modeling is usually required. To alleviate the huge computational cost, a prior thing is to speed up the solving of combustion chemistry. Different strategies [9, 10], such as DAC (Dynamic Adaptive Chemistry)[11-14], ISAT (In Situ Adaptive Tabulation) [15, 16], CCM (Chemistry Coordinate Mapping) [17], ANN (Artificial Neural Network) [18-21], and GPU acceleration [22] are adopted to reduce the direct integration (DI) time of stiff chemistry system itself. In addition to those direct acceleration methods, another brilliant idea is to extract the chemistry solving from the flow modeling by using one conserved scalar i.e. mixture fraction together with some other status variables (e.g. scalar dissipation rate, progress variable and flame front location), i.e. the flamelet concept. In flamelet model (FM), by decoupling the chemistry solving in three-dimensional (3D) space into a virtual one- (1D) or two-dimensional (2D) space coordinated by mixture fraction and status variable, detailed mechanisms with multiple species and stiff reactions can be economically employed in modeling full-scale combustors. Thus the model is extraordinary faster than finite-rate combustion models, e.g. PaSR [23, 24], EDC [25, 26] and MMC [27], which not only solve chemistry in at least multi-dimensional physical space (plus composition space for MMC) but also transport all the species involved in the kinetic mechanism(s). The applicability of flamelet model generally assumes a faster chemistry than turbulent stirring, i.e. thin reaction zone, so that the reactive scalar Y can be related to the mixture fraction ξ and status variable (usually denoted by scalar dissipation rate χ) as $Y = Y(\xi, \chi)$ in the whole flowfield. The asymptotic relation may evolve in time t as $Y = Y(\xi, \chi, t)$, i.e. unsteady flamelet. Such asymptotic relation is only valid within the thin reaction zone, where the chemistry is close to equilibrium, while outside the reaction zone the flow can be simply treated as frozen-chemistry since the fuel equivalence ratio there usually does not support combustion. However, when the turbulence becomes intense enough or the laminar flame speed S_l is lower than the eddy turnover velocity v' (Taylor-scale velocity), the asymptotic relation used in flamelet concept is not valid for the whole field any more. Under such circumstance, the flame front is convoluted to form corrugated reaction zones, and may further be broken up into distributed isolated reaction zone "islands" [28]. Strictly speaking, asymptotic relation may still exit for each fragmented flamelet (or thin reaction zone), but due to the intersection and random orientation of those fragmented flamelets no universal asymptotic relation can be derived for the ensemble of a flame region containing a large number of fragmented flamelets. In such case, flamelet based models are theoretically inapplicable and finite-rate models are usually used instead. To extend the use of FM, a new version of unsteady FM - Representative Interactive Flamelets (RIF) model [29] is proposed by Pitsch et. al., who attempt to correlate Y and ξ using the concept of representative flamelets rather than the exact asymptotic relation in the generic FM. The representative flamelet is essentially equivalent to the conditional expectation of Y on ξ adopted in CMC combustion model [30], i.e. $\langle Y|\eta = \xi \rangle$ with η the

sampling space variable, thus RIF and CMC have the same physical basis. In the following, the terminologies "representative" and "conditional" are treated as the same. And the formulation of governing equations in RIF and CMC are the same except that there is no spatial convection terms in RIF, although they are arrived at from different perspectives. Unlike FM, the applicability of RIF is not limited to thin reaction zones only, but is applicable to non-equilibrium, transient and inhomogeneous reaction processes over the whole turbulent field.

The inherent defect in the derivation of RIF lies in that the instantaneous values of Y may not be well correlated with the conserved scalar ξ for the whole field, where the actual situation may be that the data scatter around ξ with rather large fluctuations. The reason is because both the turbulence and combustion chemistry is inhomogeneous, and different turbulence-chemistry modes exist in different flame regions. Thereby, a single flamelet may not be able to actually represent the correlation between Y and ξ on the whole field. For combustion in homogeneous turbulence, such as homogeneous charge compression ignition (HCCI) combustion, RIF is especially applicable since the turbulent combustion is statistically homogeneous or the chemistry is extremely fast, i.e. there is no statistical dependence of local status on physical coordinates other than the conserved scalar and status variable(s). However, for combustion in anisotropic turbulence, which is the case in most jet fueled combustors, statistical homogeneity of Y versus ξ cannot be assumed. Thus representing the combustion chemistry of a whole flowfield by a single flamelet is not accurate anymore, because the scalars may deviate significantly from the flamelet status. Instead using the concept of local flamelets for different flow regions bearing different turbulence-chemistry interaction modes may be a more suitable solution, as long as the local statistical homogeneity can be assumed.

Hydrogen combustion has a short chemical time scale of order ~o(1) μs, implying that the turbulence-chemistry interaction is all in the flamelet regime [28] and thus the generic flamelet based models [31-33] can be used. However, such convenience cannot be enjoyed by the modeling of hydrocarbon fueled combustors. Because that hydrocarbon fuels, e.g. kerosene, usually have much larger chemical time scales of ~o(1) ms and are generally comparable to the flow time scales [34], the reaction progress strongly depends on the local turbulence mixing rate and thermophysical conditions. The generic unsteady FM uses a mean scalar dissipation rate averaged over the whole flow field, which may arise inaccuracy because the scalar dissipation rate is quite inhomogeneous in the computational domain. And also the whole-field-averaged pressure and temperature passed from the flow solver to the flamelet solver lead to errors, since the local thermophysical conditions are simply represented by global mean values.

To improve the accuracy of unsteady FM, a concept of zone flamelet is introduced here to divide the whole computational domain into several zones and the chemical status in each zone is represented by one local flamelet. With proper zone division, the scattering of variables over the mixture fraction space is in controllable small, thus the representative flamelet approaches the real scalar distribution. By using the zone flamelet, higher-resolution modeling of kerosene fueled scramjet combustor becomes available by using a mesh resolution comparable with frozen chemistry flows. The zone flamelet model is then applied to model a real supersonic combustor operated at a flight Ma (Mach number) of 6.5. The performance of zone flamelet model in highly non-equilibrium supersonic combustion is validated through comparing with measurement data. The same case configuration using finite-rate PaSR model [23, 24] is also modeled to evaluate the accuracy and computational efficiency of current zone flamelet model.

II. Governing equations

In zone flamelet model, the species are solved in a four dimensional space, i.e. the physical space and the mixture fraction space, but great computational cost can still be saved because the zone division in physical space is much coarser than the flow simulation mesh. As the zone shrinks, the stochastic variation deviating

from the representative flamelet diminishes, and thus the assumption in flamelet model is then established. The flamelet in each zone is not isolated. Across the zone boundaries, the flamelet exchange information with their neighbor zones through a flux-conserved manner, thus the flamelet variables can be transport from upstream to downstream in a flow manner.

The instantaneous equations for mixture fraction ξ and the species mass fraction Y_i are given by,

$$\frac{\partial \xi}{\partial t} + \vec{U} \cdot \nabla \xi = D\nabla^2 \xi \tag{1}$$

$$\frac{\partial Y_i}{\partial t} + \vec{U} \cdot \nabla Y_i = D\nabla^2 Y_i + W_i \tag{2}$$

with $\vec{U}$ is the velocity vector, *D* represents the diffusivity, and W_i denotes the reaction rate with unit s^{-1}. Here for simplicity, a unity Liews number is assumed. Using the concept of local representative flamelet Q_i, the instantaneous mass fraction is defined as

$$Y_i(x,t) = Q_i(\eta = \xi(x,t), x, t) + Q_i'(x,t) \tag{3}$$

where η is the sampling variable in mixture fraction space, x represents the physical coordinate, Q_i' represents the deviation of instantaneous value from the flamelet value at $\eta = \xi$. Q_i is defined as the conditional average of $Y_i(x,t)$ at $\xi(x,t) = \eta$, i.e. $Q_i = \langle Y_i | \xi(x,t) = \eta \rangle$. Thus $\langle Q_i' | \eta \rangle = 0$, and obviously the zone-averaged $\langle Q_i' \rangle_{zone} = \int \langle Q_i' | \eta \rangle P(\eta)\, d\eta = 0$, with $P(\eta)$ the probability density function (PDF) describing the distribution of ξ in the zone. As the zone shrinks, the number of sampling data points reduces, then Q_i approaches Y_i and $Q_i' \to 0$.

Differentiation of Eq. (3) gives,

$$\frac{\partial Y_i}{\partial t} = \frac{\partial Q_i}{\partial t} + \frac{\partial Q_i}{\partial \eta}\frac{\partial \xi}{\partial t} + \frac{\partial Q_i'}{\partial t} \tag{4}$$

$$\nabla Y_i = \nabla Q_i + \frac{\partial Q_i}{\partial \eta}(\nabla \xi) + \nabla Q_i' \tag{5}$$

$$D\nabla^2 Y_i = D\nabla^2 Q_i + \frac{\partial Q_i}{\partial \eta} D\nabla^2 \xi + D(\nabla \xi)^2 \frac{\partial^2 Q_i}{\partial \eta^2} + D\nabla \xi \cdot \nabla \left(\frac{\partial Q_i}{\partial \eta}\right) + D\nabla^2 Q_i' \tag{6}$$

Substituting Eq. (4)-(6) into Eq. (2), it arrives,

$$\frac{\partial Q_i}{\partial t} + \vec{U} \cdot \nabla Q_i - D(\nabla \xi)^2 \frac{\partial^2 Q_i}{\partial \eta^2} + \frac{\partial Q_i}{\partial \eta}\left(\frac{\partial \xi}{\partial t} + \vec{U} \cdot \nabla \xi - D\nabla^2 \xi\right)$$

$$+ \left(\frac{\partial Q_i'}{\partial t} + \vec{U} \cdot \nabla Q_i' - D\nabla^2 Q_i'\right) - D\nabla \xi \cdot \nabla \left(\frac{\partial Q_i}{\partial \eta}\right) - D\nabla^2 Q_i = W_i \tag{7}$$

Substituting Eq. (1) into Eq. (7), and taking the average of Eq. (7) on condition that 1) $\xi(x,t) = \eta$ and 2) within the zone $x \in zone$, it yields the final governing equation for Q_i as,

$$\frac{\partial Q_i}{\partial t} + \left\langle \vec{U} \cdot \nabla Q_i | \eta \right\rangle_{zone} + E_{ZFM} = \langle N | \eta \rangle \frac{\partial^2 Q_i}{\partial \eta^2} + \langle W_i | \eta \rangle \tag{8}$$

with $$E_{ZFM} = \left\langle \partial Q_i'/\partial t + \vec{U} \cdot \nabla Q_i' - D\nabla^2 Q_i' | \eta \right\rangle_{zone} - \langle D\nabla \xi \cdot \nabla(\partial Q_i/\partial \eta) | \eta \rangle_{zone} - \langle D\nabla^2 Q_i | \eta \rangle_{zone} \tag{9}$$

and scalar dissipation rate defined as $N = D(\nabla \xi)^2$. Here the spatial average is taken over the zone, denoted by adding a subscript "zone". Note that $\langle Q_i(\xi, x, t) | \eta \rangle_{zone} = Q_i(\eta, x, t)$ because the flamelet variable is the same within the zone. All spatial gradient of Q_i is zero within the zone except on the zone boundary, thus it arrives,

$$\left\langle \vec{U}\cdot\nabla Q_i|\eta\right\rangle_{zone}=\frac{\oiint_{zone\ boundary}\langle\vec{U}|\eta\rangle\cdot\nabla Q_i}{\oiint_{zone\ boundary}\langle\vec{U}|\eta\rangle} \tag{10}$$

which is essentially equivalent to the Gauss's flux theorem but conveniently expresses the flamelet exchange flux for irregular zones. Here, it is assumed that the velocity distribution has little similarity with the mixture fraction distribution in supersonic flows, but largely influenced by the compressibility and wave structures, thus the conditional average of velocity within η space arrives $\left\langle\vec{U}\middle|\eta\right\rangle=\vec{U}$. Following the analysis in [30], for high-Re flows, $\langle D\nabla\xi\cdot\nabla(\partial Q_i/\partial\eta)|\eta\rangle_{zone}\sim D\xi D^{-1/2}\cdot Q_i\sim D^{1/2}\sim Re^{-1/2}$, and $\langle D\nabla^2 Q_i|\eta\rangle_{zone}\sim D\cdot Q_i\sim Re^{-1}$ thus can both be neglected. Using the same closure strategy as in the generic CMC,

$$\begin{aligned}\int\left\langle\partial Q_i'/\partial t+\vec{U}\cdot\nabla Q_i'-D\nabla^2 Q_i'\middle|\eta\right\rangle_{zone}P(\eta)d\eta&=\langle\partial Q_i'/\partial t+\vec{U}\cdot\nabla Q_i'-D\nabla^2 Q_i'\rangle_{zone}\\&=\partial\langle Q_i'\rangle_{zone}/\partial t+\vec{U}\cdot\nabla\langle Q_i'\rangle_{zone}-D\nabla^2\langle Q_i'\rangle_{zone}=0\end{aligned} \tag{11}$$

In Eq. (11) the assumption of $\left\langle\vec{U}\middle|\eta\right\rangle=\vec{U}$ is also used. From Eq. (11), it seems that the effect of the first three terms in the parenthesis in Eq. (9) is to redistribute Q_i over the mixture fraction space within the zone. Observed from the DNS data [30], the conditional fluctuations Q_i' usually has the maximum at the stoichiometric mixture fraction ($\eta=\xi_{st}$), and the minimum at the two ends ($\eta=0$ & 1). Correspondingly, it is expected the terms involving conditional flucturations have a highest redistribution effect around ξ_{st}. To alleviate this redistribution effect, it is expected to control Q_i' at a lower order relative Q_i, i.e. $Q_i'\sim o(\varepsilon Q_i)$ with ε a small quantity. Thus the closure hypothesis is to neglect the first three terms in the parenthesis in Eq. (9) by assuming $Q_i'\ll Q_i$ through a fine enough zone division.

The derivation of zone flamelet model is similar to that of conditional moment closure (CMC) model [30], but the governing equations are formulated in a zone conserved form. The final equation describes the evolution of a zone based flamelet due to spatial transport, scalar diffusion and chemical reactions in the four-dimensional (4D) space. Although similar in the formula, some main differences of Eq. (8) with the CMC equations exist: 1) no conditional velocity is introduced and the conditional averaged convection term is calculated as a whole, because the correlation of velocity with mixture fraction is weak in supersonic flows. 2) the spatial convection across the zone boundary from neighbor zone(s) is calculated as a surface integral based on Gauss's theorem. 3) conditional fluctuation terms are neglected as their redistribution effect diminish as the zone division increases.

Eq. (8) is solved by Operator Splitting (OS) method. Firstly, a finite volume method is used to solve the convective part because the flamelet zone can be irregular in geometric shape and can contains random number of cells. Using The transient term and convection term are integrated over a control volume and the transient PDE in integral form is linearized as follows:

$$\frac{\rho^{n+1}Q_i^{n+1}-\rho^n Q_i^n}{\Delta t}+\frac{\Sigma_f\vec{S}_f\cdot\left(\rho\vec{U}Q_i^n\right)_f^n}{\Delta V}=0 \tag{12}$$

where n and n+1 represents the current and next-step values, f represents boundary faces, $\vec{S}_f$ is the boundary face area vector. The density ρ is added to ensure a mass conservation when across the zones. In determining the face values of Q_i^n, a simple upwind scheme is used. Secondly, the diffusion in mixture fraction space is solved by finite difference method to smooth any peaks in the Q_i distribution:

$$\frac{\partial Q_i}{\partial t}=\langle N|\eta\rangle\frac{\partial Q_i}{\partial\xi^2} \tag{13}$$

where $\langle N|\eta\rangle$ is calculated by a historical statics approach as introduced below. Finally, the chemistry is solved using the representative flamelet variables as the inputs of rate expressions,

$$\frac{\partial Q_i}{\partial t} = \langle W_i(Y_i, T)|\eta\rangle \approx W_i(Q_i, Q_T) \tag{14}$$

Such a first-order closure [30] is achieved by a Taylor expansion of the Arrhenius formula to the second order around the conditional mean, then conditionally averaging the results and neglecting all the conditional fluctuation terms.

The flamelet temperature Q_T influences the reaction progress in each mixture fraction space represented by a flamelet. In addition to solving the flamelet or conditional temperature equations, various algebraic models has been proposed, e.g. the enthalpy defect/excess model [35-43] and Conditional Source-term Estimation (CSE) [44, 45]. Here, the representative flamelet temperature is not solved from its flamelet equation, mainly to avoid the complex construction of sub-models in the flamelet space for various heat additions or sinks, such as the viscous dissipation, the radiation and the wall heat loss.

Ignoring the enthalpy defect fluctuations ($H' \sim o(0)$) [42], and therefore the corresponding PDF distribution of $\langle H|\eta\rangle$ is assumed to be a Dirac delta function centered on the local mean value of the enthalpy $\widetilde{H}$. then $\langle H|\eta\rangle$ can be estimated using an approach of historical statistics,

$$\langle H|\eta\rangle = \left\langle \widetilde{H}\middle|\tilde{\xi} = \eta\right\rangle = \frac{1}{n}\sum_{t_{n-i}}^{t_n}\left\langle \widetilde{H}\middle|\tilde{\xi} = \eta\right\rangle \tag{15}$$

where n is the number of sampling data points with the condition $\tilde{\xi} = \eta$. Generally, the time sampling window $\Delta t = t_n - t_{n-i}$ should not span too many time steps, in order to reflect the latest temperature field. Such a statistical enthalpy approach mimics the enthalpy defect/excess model [35, 36] but provides a more reasonable estimation of the enthalpy defect/excess status in each zone. Then the flamelet temperature can be calculated as a function of conditional enthalpy and flamelet mass fractions $Q_T = f(\langle H|\eta\rangle, Q_i)$. The current historical statistics approach also significantly saves the computational cost in directly solving the flamelet temperature equation with numerous sub-models needed to be included for real combustor cases.

Similarly, the conditional scalar dissipation rate $\langle N|\eta\rangle$ is estimated by the same historical statistics approach to approximate its distribution in the mixture fraction space,

$$\langle N|\eta\rangle = \frac{1}{n}\sum_{t_{n-i}}^{t_n}\left\langle \widetilde{N}\middle|\tilde{\xi} = \eta\right\rangle \tag{16}$$

The β-function PDF is used in this study because of its continuous shape for integration and the implication of δ-function in its expression. $P(\eta)$ is given as a function of the mean mixture fraction $\tilde{\xi}$ and its variance $\widetilde{\xi''^2}$. Favre mean equations for $\tilde{\xi}$ and $\widetilde{\xi''^2}$ are respectively solved from their governing equations [46]. The Favre mean species mass fractions $\widetilde{Y_i}$ are recovered by Favre PDF weighted integration,

$$\widetilde{Y_i} = \int Q_i P(\eta) d\eta \tag{17}$$

and then Favre mean temperature $\tilde{T}$ is obtained given $\widetilde{H}$ and $\widetilde{Y_i}$.

Generally, there can be two types of zone division methods. One is to divide the computation domain simply according to the geometric shape and the global flow pattern, and the other is to dynamically divide the domain according to the local flow pattern. In this study, the simple geometric division is adopted, and the domain is divided into 40 slices from the upstream entrance to the downstream outlet by considering that fuel of the same residence time shares approximately the same conditional flame structure. In the future study, the dynamic zone division based on mixture fraction or scalar dissipation rate will be tested and evaluated.

III. Numerical implementation

The Favre-filtered or Favre-averaged Navier–Stokes equations governing a mixture of thermally perfect gases are solved together with the transport equations for species and absolute enthalpy. Thermodynamic curve fitted from McBride et al. JANAF thermophysical properties[47] are used for species-specific heats and

enthalpies. Sutherland formula [48] and Wilke's law [49, 50] are used to calculate the molecular viscosity of multicomponent mixture. The mixture thermal coefficient is obtained assuming a constant Prandtl number of 1.0. Molecular diffusion processes are described by Fick's law, parameterized by a constant Schmidt number of 1.0.

A. Experimental case

Supersonic combustion in the elliptical combustor is tested in a continuous-flow supersonic combustion test facility. The vitiated air heater provides high-enthalpy incoming flow through burning hydrogen with oxygen replenishment in air stream. Liquid kerosene heated to supercritical status by an electric ceramic heater is delivered to the test article. The scramjet combustors are composed of three sections: a 600-mm-long isolator section with a slight 0.7 ° divergence angle, an 800-mmm-long burner section, and a 600-mm-long expander section with a large 4 °divergence angle. There are two circumvented cavities assembled in tandem in the burner section for the purpose of flame anchoring and possibly re-ignition. Both the cavities have a depth of 15 mm and a length-depth ratio of 7. The aft walls of the cavities are at an angle of 45 ° relative to the cavity floor. Supercritical kerosene is injected through 6 circumferential injection portholes with the diameter of 2.5 mm. Static pressure is measured by Motorola MPX2200 pressure transducers along the inner wall of the combustor assembly all with 50 mm intervals.

In the test case, the incoming vitiated air has a Ma of 3.0, a raised stagnation temperature of 1600 K and a mass flow rate of 3.6 kg/s at the isolator entrance, which are set to simulate a flight Ma of 6.5. The compositions of vitiated air are N_2 in 60.5% mole fraction, O_2 in 21.7% and H_2O in 17.8%. The global fuel equivalence ratio is 0.8 (symbolized by Φ). The total pressure and temperature of supercritical kerosene is 5.77 MPa and 784 K respectively. The combustor is not protected by any recirculating water-cooling system, however no significant damage to the wall surface after the test duration of approximately 27 s, suggesting that the wall temperature is still within the thermal limit (~ 1300 K) of the wall material.

B. Turbulence closure

The traditional Boussinesq hypothesis is used to relate unresolved turbulent stresses to the rate of strain of the resolved velocity field by equally treating the turbulent viscosity in RANS (Reynolds-Averaged Navier-Stokes) and the subgrid scale (SGS) viscosity in LES. Gradient diffusion models parameterized by constant Prandtl (1.0) and Schmidt (1.0) numbers are used to account for the heat and mass fluxes due to unresolved turbulent eddies. Closure of the SGS stress tensor and scalar fluxes is accomplished by specifying an eddy viscosity to simulate both the subgrid-scale and near-wall turbulence effects. Improved Delayed Detached Eddy Simulation (IDDES) [51, 52] is employed in this study to enable an automatic choice of RANS or LES mode depending on the local boundary layer thickness and turbulent viscosity. In IDDES, when the non-dimensional normal wall distance becomes excessively large, a so-called wall modeled LES (WMLES) branch will be activated to directly bridge the viscosity-affected sublayer (VASL) between the wall and the logarithmic layer, through acting as a semi-empirical wall function to model the wall stress in the first off-wall points in the logarithmic layer. In comparison with previous studies [53-55] conducted by the authors' group, the application of IDDES apparently weakens the influence of near-wall meshing on the internal flow fields.

In a comparative case, the effect of micro-mixing due to unresolved eddies on chemical reaction rate is modeled by PaSR model, where the final reaction rate ω_t is mutually determined by the characteristic time scales of chemical reactions τ_c and turbulent micro-mixing τ_{mix},

$$\omega_t = \omega_l \frac{\tau_c}{\tau_c + \tau_{mix}} \tag{18}$$

where ω_l is the reaction rate over the current integration time step, τ_{mix} is the micro-mixing time scale, and $C_{\mathrm{mix}} = 1.0$. In PaSR, the micro-mixing time scale τ_{mix} is on the same order of magnitude of Kolmogorov time scale τ_{k}, $\tau_{\mathrm{mix}} = C_{\mathrm{mix}}\left(\frac{\nu_{\mathrm{eff}}}{\epsilon}\right)^{1/2} \sim o(\tau_{\mathrm{k}})$ with $C_{\mathrm{mix}} = 1.0$. In the S-A based DES, the SGS turbulent kinetic energy k_{sgs} and it dissipation rate ϵ are estimated from their relationships with SGS eddy viscosity ν_t, i.e. $k_{sgs} = (\nu_t/(c_k d_{DDES}))^2$ and $\epsilon = 2\nu_{eff}|S_{ij}|^2$, with $c_k = 0.07$ and S_{ij} is the strain rate. The overall chemical time scale is estimated as the summation ratio of species concentrations to reaction rates $\tau_c = \sum c_i / \sum \omega_i$.

In the serial studies conducted by the authors' group, the detailed kerosene mechanism proposed by Dagaut et al. [56] is reduced under the typical working condition range of scramjet combustors, i.e. equivalence ratio of 0.6-1.4, static pressure of 0.5-3.0 bar, and static temperature of 300-3000 K. Till now, four versions of skeletal mechanisms, respectively 48s/197r [55], 39s/153r [53, 54], 28s/92r [34] and current 19s/54r [57], have been developed from the original 2815s/8217r mechanism [56] by using a highly efficient and reliable directed relation graph with error propagation and sensitivity analysis (DRGEPSA) method [58] in together with manual path analysis. Although the mechanism size has been significantly reduced, the key kinetic properties such as adiabatic flame temperature, heat release rate, ignition delay and laminar flame speed agree well with the original detailed mechanism. In this study, the latest version of reduced RP-3 mechanism with species number of 19 and reaction number of 54 will be used in the combustion models.

C. Numerical details

The modeling is performed by the compressible reacting flow solver AstroFoam, which is developed on the basis of the compressible flow solver rhoCentralFoam distributed with OpenFOAM V3.0.1 CFD package [59] mainly through adding the features of multi-species transport and multi-component reaction. AstroFoam together with the original rhoCentralFoam solver was firstly validated for various frozen flows, including the canonical shock tube problem, forward step flow, hypersonic flow over a boconic and supersonic jets [60-63]. The solver is then applied for various scramjet combustor cases [34, 54] to examine its accuracy and robustness in the engineering modeling of supersonic combustion.

The governing equations for momentum, species and energy are solved explicitly for the advection and implicitly for the other processes by using operator splitting (OS) method. Explicit systems formulated as $Ax=b$ (A is the coefficient matrix, x is the unknown variable field, and b is the source term field) involve only diagonal terms of matrix A ($A.diag$) and can be directly solved by the diagonal solver as $x=b/A.diag$. For implicit systems, the large sparse matrixes are solved by conjugate gradient solvers preconditioned by diagonal incomplete-Cholesky factorization for symmetric matrixes (those without advective terms) and incomplete-LU factorization for asymmetric matrixes.

First-order implicit Euler method is used for the temporal marching, while second-order spatial difference is achieved by using the TVD (Total Variation Diminishing) [64] or (NVD) Normalized Variable Diagram (NVD) [65] interpolation scheme with appropriate flux limiter. Those second order flux limiters are designed to pass through a certain region of the solution, known as the TVD region, in order to guarantee the scheme stability. Figure 1 compares some common flux limiters on the TVD region. As seen, the TVD-type Minmod limiter and the NVD-type SFCD limiter overlap with each other, and thus have equivalent interpolation accuracy. The Superbee has the minimum numerical viscosity among the second order limiters, and correspondingly the least numerical instability. When the parameter of the Gamma differencing limiter decreases from 1 to 0, its numerical dissipation reduces to 0 since the scheme itself becomes the central scheme,

but its numerical dispersion rises significantly. The vanLeer limiter is identical to the Gamma 1 limiter for $r < 1$ (r - successive gradient ratio), but drifts towards the backward difference for $r > 1$. In our numerical tests of supersonic combustor modeling, the Superbee and Gamma 0 limiters show the worst numerical stability since large flow gradients and discontinuities are fully filled in the supersonic combustion fields. While the vanLeer and the Gamma 1 limiters occasionally lead to divergence due to unphysical interpolation values, e.g. negative density or infinite large flow speed. Generally, the Minmod and SFCD limiters show the best numerical stability while acceptable numerical dissipation for capturing the main eddy features in the combustor, and are thus used in current case calculations.

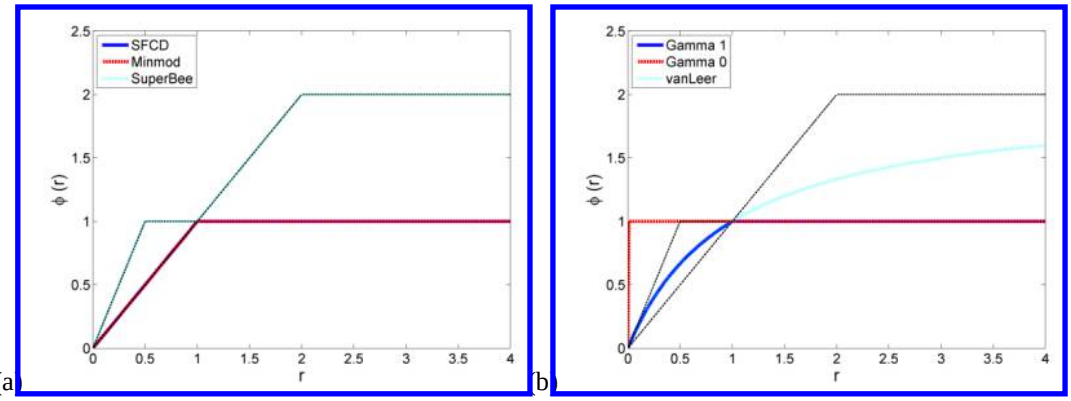

(a) (b)

Figure 1. Limiter functions overlaid onto second-order TVD region (enclosed by the black dashed lines); r represents the ratio of successive gradients on the solution mesh, and the limiter function is constrained to be $\boldsymbol{\phi(r) \geq 0}$

The computational domain contains the isolator, burner and expander sections. Due to the bilateral symmetry of the combustors, quarterly split domain is modeled with symmetrical boundary condition applied to the splitting planes. The whole domain is firstly meshed by using Cartesian CutCell method with uniform 1 mm cells, which are then adaptively refined based on the local curvature and size function. Away from the boundary layer, the minimum cell size is 0.125 mm, which is mainly distributed around the fuel injectors. The first near-wall cell height in the inflation layer is 5 μm, which corresponds to a non-dimensional cell size y^*<1 on all the wall surfaces for the examined combustor flows. The total cell number in the split combustor domain is 27.4 million for the elliptical combustor. In the following analysis, the coordinate origin locates at the lower left corner of the isolator inlet plane viewed from outside, with X, Y and Z respectively represent the streamwise, height and spanwise directions.

Fixed pressure, temperature and velocity on the isolator inlet and the fuel inlets are set as the same as the test configurations. Open boundary condition is applied to the expander outlet, where zero gradient is used for outflow and ambient flow conditions for temperature and gas composition are specified should backflow occur. Inner wall temperature along the streamwise direction is specified linearly from 500 K at the isolator entrance to 1200 K at the expander outlet.

The computations are performed in parallel at national supercomputer center in Tianjin (TH-1) using 240 CPU cores. The total calculation time is 150,000 CPU hours for the PaSR modeling, while only around 10% for the modeling based on zone flamelet. Each modeling case was running with 3 flush through times (FTTs) for data sampling and statistics.

IV. Results and discussion

Figure 2 compares the time-averaged streamwise static pressure on the ensemble wall predicted respectively by PaSR and current zone flamelet model. The measurements were repeated for three times to ensure the data

reliability. The predictions by PaSR and zone flamelet are similar, and both agree well with the measurements. The peak pressure rise ratio (the ratio of maximum pressure to the inlet pressure $P_{max}/P_{inlet} \approx 3.8$) and initial pressure rise location are both correctly predicted, and the general trends are also well predicted by the two models. The major difference between the predictions and the measurements lie in the sharper initial pressure rise at the beginning. The pressure profiles on the descending side are similar with each other and almost identical to the measurements. The pressure valley immediately before the downstream cavity, which cannot be observed in current coarser measurements, needs to be validated in the future experiment through laying more pressure transducers there.

Figure 3 shows the basic flow structures visualized by numerical shadowgraph. The location and wave structures of shock train in the isolator are rather similar for the predictions by PaSR and zone flamelet. The interaction of shock waves from the opposite walls belongs to Type I shock-shock interference [66]. The shock train is enveloped by a drum-shape detached boundary layer. Also the bow shock attached to the fuel jet immediately out of the porthole can be observed. The unburnt fuel jet extends till the end of the upstream cavity for the PaSR case, while a much shorter unburnt fuel jet extends only to the leading edge of upstream cavity for the zone flamelet case. Another important difference is that the plume structures of hot combustion gas layer are in larger scale yet irregular for the zone flamelet case, while finer yet more uniform for the PaSR case.

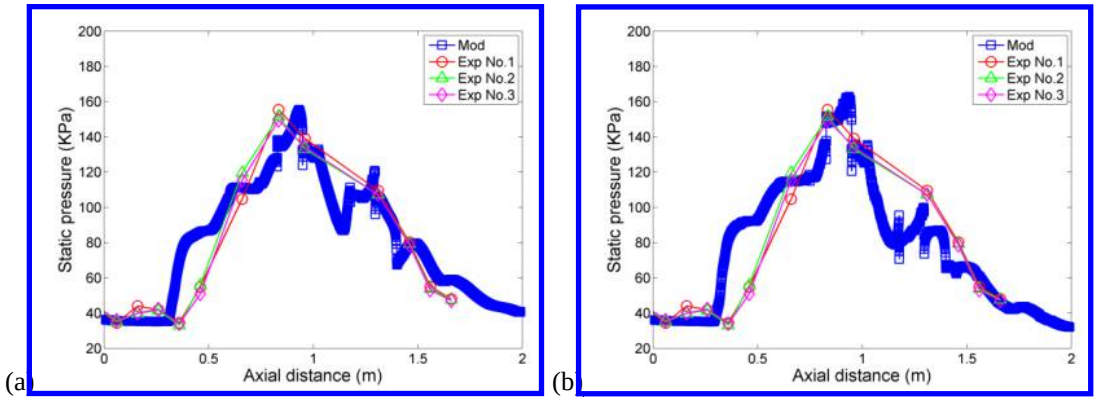

Figure 2. Comparisons of predicted time-averaged static pressure with the measurements for the (a) PaSR and (b) Zone flamelet modelings

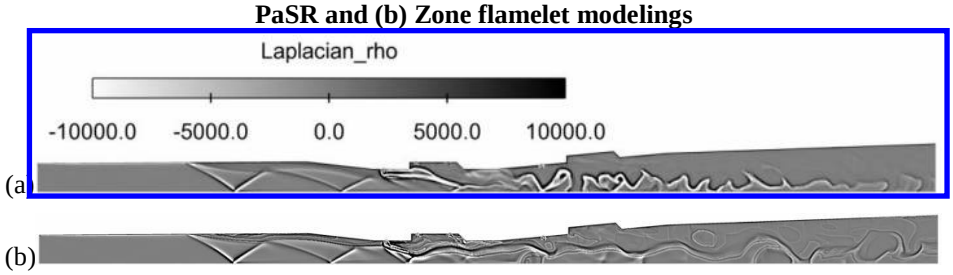

Figure 3. Instantaneous fields for numerical shadowgraph (Laplacian of the density field) on the clip planes through one injector, predicted by (a) PaSR and (b) zone flamelet

The time-averaged Ma (Mach number) fields shown in Figure 4 indicate that the distribution of subsonic regions are quite similar for the two modeling cases, i.e. attached to the shock train and the two cavities. The sizes of subsonic regions are also similar, with a slightly larger one attached to the upstream cavity for the zone flamelet case, and small spots of subsonic regions along the combustor axis after each pseudo shock wave can be observed. The Ma in the expander is higher for the zone flamelet case but the mean flow speed are almost the same, this can be explained by the lower mean temperature and thus lower sonic speed there.

From Figure 5, the most obvious difference shown by the instantaneous temperature fields is the flame stabilization mode [4], which is the cavity mode for the PaSR case while the jet wake mode for the zone

flamelet mode. And as pointed out in Figure 3, the coherent flame structures is in larger scale yet irregular for the zone flamelet modeling, this is mainly because the heat release is more concentrated in zone flamelet mode while more distributed in the full-transport and finite-rate PaSR model. In zone flamelet model, the local heat release is closely conditioned by the mixture fraction and apparently more intense around the iso-surface of stoichiometric mixture fraction. From the time evolution of instantaneous temperature fields in the PaSR case, the upstream cavity acts as a constant igniter, where the flame is intermittent, and the downstream cavity acts as a flame holder, where the flame resides there all the time. Hereby the mean temperature around the downstream cavity is 100-200 K higher for the PaSR case. In the zone flamelet case, the flame always resides in the thin mixing layer above the two cavities.

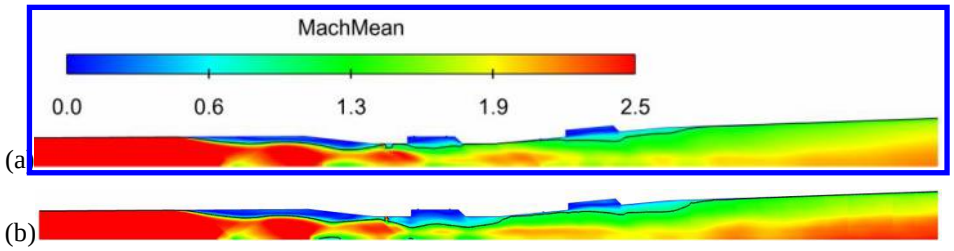

Figure 4. Time-averaged Ma fields on the clip planes through one injector, predicted by (a) PaSR and (b) zone flamelet

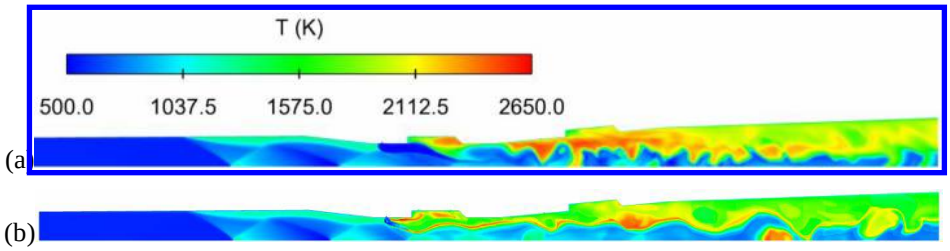

Figure 5. Instantaneous temperature fields on the clip planes through one injector, predicted by (a) PaSR and (b) zone flamelet

The distributions of mixture fraction (denoted as ξ) in Figure 6 are generally similar for the two models, i.e. the mixing or dispersion of fuel is mainly finished before the end of upstream cavity with ξ decreases quickly to below 0.3. Another observation is that the jet penetration is lower for the zone flamelet case, probably because the reaction on the upwind side of the fuel jet quickly decreases the local Ma thus significantly reduces the jet momentum flux. While for the PaSR case, there is little reaction on the upwind side. Usually, the mixing performance is accessed in frozen-chemistry condition in the design of a supersonic fuel injector, while little attention is paid to examine the influence of combustion on the mixing. The reactions decrease the local Ma through two main mechanisms, 1) increasing the gas constant $R = R_u/MW$, where R_u is the universal gas constant and MW is the molecular weight, by pyrolyzing the large-molecule hydrocarbon fuel(s) into more small-molecule hydrocarbons (e.g. CH_3, C_2H_4); 2) increasing the temperature by exothermic reactions. That means fierce reactions may not always be helpful in improving the combustion efficiency but rather may decrease it through decreasing the jet penetration and then macro-mixing. This is the reason why applying global mechanisms or assuming equilibrium chemistry may significantly underpredict the pressure rise ratio. Thus in the design of supersonic injectors, it would be beneficial to suppress the reactions in the jet foot to maintain a high momentum flux and increase the jet penetration height.

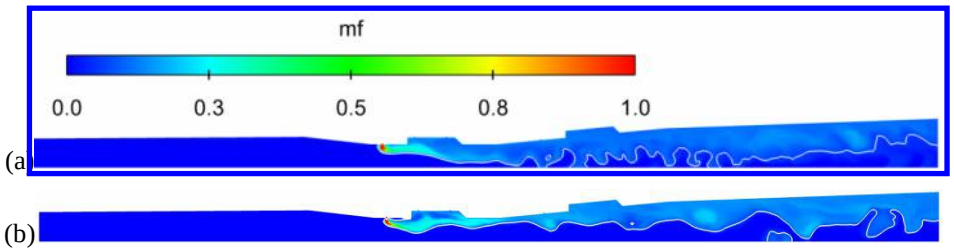

Figure 6. Instantaneous mixture fraction fields on the clip planes through one injector, predicted by (a) PaSR and (b) zone flamelet; the solid white line denotes stoichiometric condition (ξ=0.068)

Figure 7 compares the distributions of CO, H_2O and OH predicted by PaSR and zone flamelet. CO is formed since the jet wake in the zone flamelet case, while the formation of CO only starts since the upstream cavity in the PaSR case. The CO distribution clearly indicates the two-layer flow pattern, i.e. the upper hot combustion gas layer and the beneath cold crossflow layer. CO almost fully fills the expander since the downstream cavity in both cases. The coherent plume structures are obviously in larger scale for the zone flamelet case, probably because the chemistry is represented globally by a single flamelet in each zone. H_2O is formed in the cavity and/or shear/mixing layer and then accumulated in the expander. The difference between zone flamelet and PaSR modellings is that there is little reaction (indicated by H_2O formation) in the shear/mixing layer, while reactions start since the upwind side of the fuel jet till the downstream shear/mixing layer, forming a jet-wake flame stabilization mode. The OH distribution can be considered as an indicator of the actual reaction zones, which are distributed mainly in a thick mixing layer after the upstream cavity for the PaSR case and a much thinner shear/mixing layer since the jet wake for the zone flamelet case. This is because the flamelet based models identify the reaction zones only by the local mixture faction, thus the upwind shear/mixing layer with stoichiometric iso-surface embedded inside is considered to have the same reaction status as that on the leeward side (i.e. inside the cavity). One of the main drawback of flamelet based modes is that they do not distinguish the two sides of a jet, which is reasonable for axial jet flames but may incorrectly ignite the upwind side for transverse jet flames. A future model correction should be made to improve the prediction near the jet root.

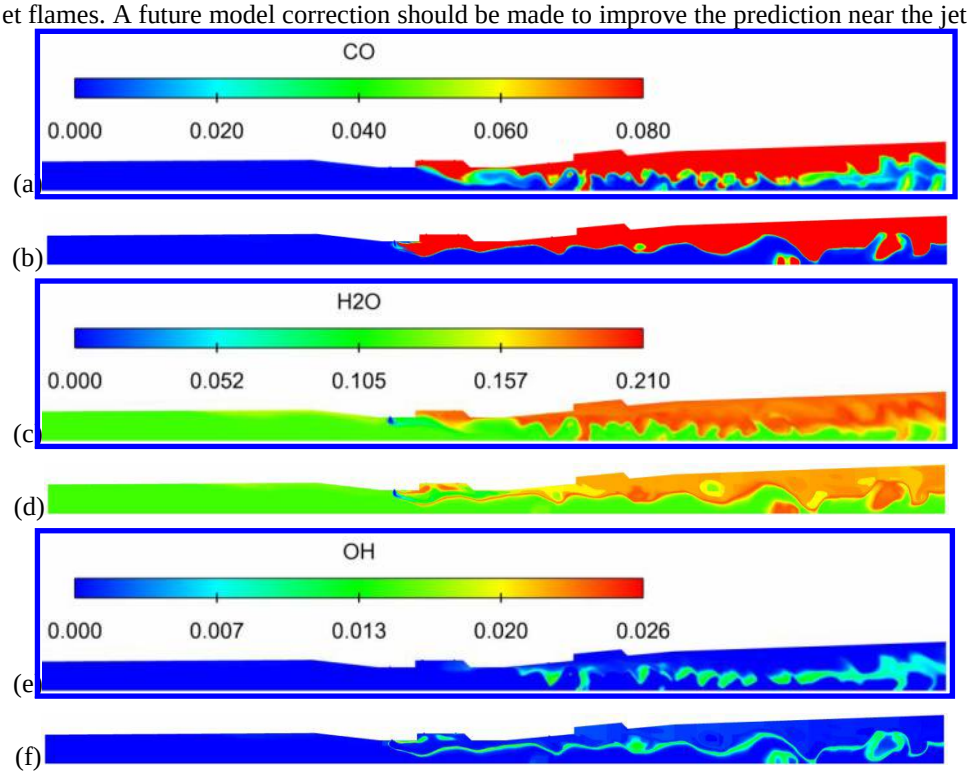

Figure 7. Instantaneous mass fraction fields of (a-b) CO, (c-d) H_2O and (e-f) OH on the clip planes through one injector, predicted by (up) PaSR and (down) zone flamelet

Compared with the PaSR modelling with full-transport and finite-rate stiff chemistry modeling, the current zone flamelet modeling significantly reduces the computational cost by at least one order of magnitude, i.e. the chemistry solving time in the zone flamelet modeling is only 10% of that in the PaSR modeling. Apart from the flow modeling part, the solving of combustion chemistry requires a total of 27.4 million (i.e. the element number) direct integrations (DIs). While the zone flamelet modeling requires only $N_{zone} \times N_{\xi}$ (N_{zone} - number of zone division, N_{ξ} - grid number in the mixture fraction space) DIs. In this current study, a total of N_{zone}=40 zones are divided simply according to the combustor geometry, and a grid with N_{ξ}=100 and clustering around the stoichiometric mixture fraction is meshed in the mixture fraction space. Thus the times of DIs are significantly reduced to 1.5% in the zone flamelet modeling relative to the PaSR modeling. Furthermore, considering only the transport of mixture fraction and its variance are solved in the zone flamelet modeling while the full transports of all the species are solved in the PaSR modeling, the time saving in scalar transport is also substantial. Due to the use of ISAT technique, the computational time of stiff chemistry in the PaSR and zone flamelet cases are both significantly saved. But still the zone flamelet coupled with ISAT shows an 10-fold increase in the computational efficiency of combustion chemistry than the PaSR with ISAT.

V. Conclusions

A novel zone flamelet model is proposed in this study to alleviate the computational cost in supersonic combustor modeling and to better represent the local turbulence-chemistry interaction. To account for the different turbulence-chemistry modes existing in inhomogeneous turbulent combustion, e.g. most jet-fueled combustors, the concept of local flamelets for different flow regions is proposed by assuming local statistical homogeneity of Y versus ξ. The zone flamelet is developed through dividing the whole computational domain into a number of control zones and the chemical status in each zone is represented by one local flamelet. With proper zone division, the local flow conditions can be assumed to be homogeneous, where the scattering of variables over the mixture fraction space is in controllable small, thus the representative flamelet approaches the real scalar distribution. The flamelets exchange information with the neighbor zones through a flux-conserved manner when across the zone boundary, thus the flamelet variables can be transport from upstream to downstream in a flow manner.

The zone flamelet is similar with the traditional CMC model, but the governing equations are formulated in a zone conserved form. Some major differences are: 1) mean velocity is used instead of conditional velocity; 2) spatial convection across the zone boundary is calculated as a surface integral; 3) conditional fluctuation terms are neglected. To avoid the construction of sub-models in the flamelet space for various non-adiabatic terms (e.g. viscous dissipation, radiation and wall heat loss) and further reduce the computational cost, the representative flamelet temperature is calculated based on a historical statistics of total enthalpy in each zone over the mixture fraction space, rather than resolving from its flamelet equation.

The zone flamelet model is then applied to model a real supersonic combustor operated at a flight Ma (Mach number) of 6.5, and compared with finite-rate PaSR. Both the initial pressure rise location and the peak pressure rise ratio of time-averaged pressure are well predicted by zone flamelet and PaSR. And the overall pressure profiles predicted by the two models are close. The location and wave structures of shock train in the isolator are rather similar for the predictions by PaSR and zone flamelet. The most obvious difference is the flame stabilization mode, which is the cavity mode for the PaSR case while the jet wake mode for the zone flamelet mode. This is due to the inherent drawback of flamelet based modes as they do not distinguish the two sides of a

jet, which is reasonable for axial jet flames but may incorrectly ignite the upwind side for transverse jet flames. In addition, The coherent flame structures is in larger scale yet irregular for the zone flamelet modeling, this is mainly because the heat release is more concentrated in zone flamelet mode while more distributed in the full-transport and finite-rate PaSR model. A future model correction should be made to improve the prediction near the jet root.

Compared with the PaSR modelling coupled with ISAT, the current zone flamelet modeling coupled with ISAT significantly reduces the computational cost by at least one order of magnitude, i.e. the chemistry solving time in the zone flamelet modeling is only 10% of that in the PaSR modeling. This is mainly because the time of direct integrations (DIs) and scalar transports are significantly saved in zone flamelet model.

Acknowledgments

The Project was supported by National Natural Science Foundation of China (Grant No. 11502270) and Training Program of the Major Research Plan of the National Natural Science Foundation of China (Grant No. 91641110). The authors are also grateful to National Supercomputer Center in Tianjin for providing computational resource.

Reference

1. Cutler, A. D., Magnotti, G., Cantu, L., Gallo, E., Rockwell, R., and Goyne, C. "Dual-Pump Coherent Anti-Stokes Raman Spectroscopy Measurements in a Dual-Mode Scramjet", *Journal of Propulsion and Power*, 30 (3), 2014, 539-549.
2. O'Byrne, S., Danehy, P. M., Cutler, A. D., and Tedder, S. A. "Dual-Pump Coherent Anti-Stokes Raman Scattering Measurements in a Supersonic Combustor", *AIAA Journal*, 45 (4), 2007, 922-933.
3. Luca, C., Emanuela, G., Andrew, D. C., Brett, F. B., Paul, M. D., Robert, D. R., Christopher, P. G., and James, C. M. "Nitric Oxide PLIF Visualization of Simulated Fuel-Air Mixing in a Dual-Mode Scramjet (Invited)", *53rd AIAA Aerospace Sciences Meeting*. AIAA 2015-0354, American Institute of Aeronautics and Astronautics, Kissimmee, Florida, 2015.
4. Yuan, Y., Zhang, T., Yao, W., and Fan, X. "Distributions of Flame Stabilization Modes in Supersonic Combustor", *36th International Symposium on Combustion*. Seoul, Korea, 2016.
5. Yuan, Y., Zhang, T., Yao, W., and Fan, X. "Study on Flame Stabilization in a Dual-Mode Combustor Using Optical Measurements", *Journal of Propulsion and Power*, 31 (6), 2015, 1524-1531.
6. Clark, R. J., and Shrestha, S. O. B. "Review of numerical modeling and simulation results pertaining to high-speed combustion in scramjets", *49th AIAA/ASME/SAE/ASEE Joint PropulsionConference*. AIAA 2013-3724, American Institute of Aeronautics and Astronautics, San Jose, California, 2013.
7. Drummond, J. P. "Development of Methods to Predict High-Speed Reacting Flows in Aerospace Propulsion Systems", *50th AIAA Aerospace Sciences Meeting including the New Horizons Forum and Aerospace Exposition*. American Institute of Aeronautics and Astronautics, 2012.
8. Ingenito, A., De Flora, M. G., and Bruno, C. "LES Modeling of Scramjet Combustion", *44th AIAA Aerospace Sciences Meeting and Exhibit*. Reno, 2006.
9. Imren, A., and Haworth, D. C. "On the merits of extrapolation-based stiff ODE solvers for combustion CFD", *Combustion and Flame*, 174, 2016, 1-15.
10. Lu, T., and Law, C. K. "Toward accommodating realistic fuel chemistry in large-scale computations", *Progress in Energy and Combustion Science*, 35 (2), 2009, 192-215.

11. Contino, F., Jeanmart, H., Lucchini, T., and D'Errico, G. "Coupling of in situ adaptive tabulation and dynamic adaptive chemistry: An effective method for solving combustion in engine simulations", *Proceedings of the Combustion Institute*, 33 (2), 2011, 3057-3064.
12. Liang, L., Stevens, J. G., and Farrell, J. T. "A dynamic adaptive chemistry scheme for reactive flow computations", *Proceedings of the Combustion Institute*, 32 (1), 2009, 527-534.
13. Pepiot-Desjardins, P., and H.Pitsch. "An efficient error-propagation-based reduction method for large chemical kinetic mechanisms", *Combustion and Flame*, 154, 2008, 67-81.
14. Lu, T., and Law, C. K. "Linear time reduction of large kinetic mechanisms with directed relation graph: n-Heptane and iso-octane", *Combustion and Flame*, 144 (1-2), 2006, 24-36.
15. Pope, S. B. "Computationally efficient implementation of combustion chemistry using in situ adaptive tabulation", *Combustion Theory and Modeling*, 1, 1997, 41-63.
16. Yang, B., and Pope, S. B. "Treating chemistry in combustion with detailed mechanisms - In situ adaptive tabulation in principal directions - premixed combustion", *Combustion and Flame*, 112, 1998, 85-112.
17. Jangi, M., and Bai, X.-S. "Multidimensional chemistry coordinate mapping approach for combustion modelling with finite-rate chemistry", *Combustion Theory and Modelling*, 16 (6), 2012, 1109-1132.
18. Baris, S., and Suresh, M. "Artificial Neural Networks Based Chemistry-Mixing Subgrid Model for LES", *47th AIAA Aerospace Sciences Meeting including The New Horizons Forum and Aerospace Exposition*. AIAA 2009-241, American Institute of Aeronautics and Astronautics, Orlando, Florida, 2009.
19. Baris, S., and Suresh, M. "Representation of Chemical Kinetics by Artificial Neural Networks for Large Eddy Simulations", *43rd AIAA/ASME/SAE/ASEE Joint Propulsion Conference & Exhibit*. American Institute of Aeronautics and Astronautics, 2007.
20. Rajat, K., Vaidyanathan, S., and Suresh, M. "Towards Engineering Les of Reacting Flows:Artificial Neural Networks for Efficient Kinetics Modeling", *41st Aerospace Sciences Meeting and Exhibit*. AIAA 2003-311, American Institute of Aeronautics and Astronautics, Reno, Nevada, 2003.
21. Chen, J. Y., Blasco, J. A., Fueyo, N., and Dopazo, C. "An economical strategy for storage of chemical kinetics: Fitting in situ adaptive tabulation with artificial neural networks", *Proceedings of the Combustion Institute*, 28 (1), 2000, 115-121.
22. Niemeyer, K. E., and Sung, C.-J. "Accelerating moderately stiff chemical kinetics in reactive-flow simulations using GPUs", *Journal of Computational Physics*, 256, 2014, 854-871.
23. Golovitchev, V. I., and jarnicki, R. "Numerical modeling of high temperature air "flameless" combustion", *The 4th International Symposium on High Temperature Air Combustion and Gasification*. Rome, Italy, 2001.
24. Golovitchev, V. I., Nordin, N., Jarnicki, R., and Chomiak, J. "3-D Diesel Spray Simulations Using a New Detailed Chemistry Turbulent Combustion Model", *CEC/SAE Spring Fuels & Lubricants Meeting & Exposition*. Paris, France, 2000.
25. Magnussen, B. F. "On the Structure of Turbulence and a Generalized Eddy Dissipation Concept for Chemical Reaction in Turbulent Flow", *19th American Institute of Aeronautics and Astronautics Aerospace Science Meeting*. St. Louis, Missouri, 1981.
26. Magnussen, B. F. "The Eddy Dissipation Concept: A Bridge Between Science and Technology", *ECCOMAS Thematic Conference on Computational Combustion*. Lisbon, Portugal, 2005.
27. Vogiatzaki, K., Kronenburg, A., Cleary, M. J., and Kent, J. H. "Multiple mapping conditioning of turbulent jet diffusion flames", *Proceedings of the Combustion Institute*, 32 (2), 2009, 1679-1685.
28. Ingenito, A., and Bruno, C. "Physics and Regimes of Supersonic Combustion", *AIAA Journal*, 48 (3), 2010, 515-525.

29. Pitsch, H., Wan, Y. P., and Peters, N. "Numerical Investigation of Soot Formation and Oxidation Under Diesel Engine Conditions". SAE International, 1995.
30. Klimenkoa, A. Y., and Bilger, R. W. "Conditional momen closure for turbulent combustion", *Progress in Energy and Combustion Science,* 25, 1999, 595-687.
31. Peters, N. "Laminar flamelet concepts in turbulent combustion", *Twenty-first Symposium (International) on Combustion*. Pittsburgh, Pennsylvania, 1986, 1231-1250.
32. Pitsch, H., Chen, M., and Peters, N. "Unsteady flamelet modeling of turbulent hydrogen-air diffusion flames", *27th Symposium (International) on Combustion,* 27 (1), 1998, 1057-1064.
33. Bourlioux, A., and Volkov, O. "Validation of unsteady flamelet models for non-premixed turbulent combustion with intermittency", *Proceedings of 11th Annual Conference of the CFD society of Canada*. Vancouver, British Columbia, 2003, 431-436.
34. Yao, W., Lu, Y., Li, X., Wang, J., and Fan, X. "Improved Delayed Detached Eddy Simulation of a high-Ma active-cooled scramjet combustor based on skeletal kerosene mechanism", *52nd AIAA/SAE/ASEE Joint Propulsion Conference*. Salt Lake City, Utah, 2016, AIAA-2016-4761.
35. Cleary, M., and Kent, J. "Modelling of species in hood fires by conditional moment closure", *Combustion and Flame,* 143 (4), 2005, 357-368.
36. Young, K. J., and Moss, J. B. "Modeling sooting turbulent jet flames using an extended flamelet technique", *Combustion Science and Technology,* 105, 1995, 33-53.
37. Brookes, S. J., and Moss, J. B. "Predictions of soot and thermal radiation properties in confined trubulent jet diffusion flames", *Combustion and Flame,* 116, 1999, 486-503.
38. Kennedy, I. M., Kollmannt, W., and Ghen, J. Y. "Predictions of soot in laminar diffusion flames", *AIAA Journal,* 29 (9), 1991, 1452-1457.
39. Bai, X. S., Balthasar, M., Mauss, F., and Fuchs, L. "Detailed soot modeling in turbulent jet diffusion flames", *Twenty-Seventh Symposium (International) on Combustion*. 27, The Combustion Institute, Colorado, 1998, 1623-1630.
40. Louis, J. J. J., Kok, J. B. W., and Klein, S. A. "Modeling and measurements of a 16-kw turbulent nonadiabatic syngas diffusion flame in a cooled cylindrical combustion chamber", *Combustion and Flame,* 125, 2001, 1012-1031.
41. Kim, G., Kang, S., Kim, Y., and Lee, K.-S. "Conditional moment closure modeling for a three-dimensional turbulent non-premixed syngas flame with a cooling wall", *Energy and Fuels,* 22, 2008, 3639-3648.
42. Cuoci, A., Frassoldati, A., Faravelli, T., and Ranzi, E. "Kinetic Modeling of Soot Formation in Turbulent Nonpremixed Flames", *Environmental Engineering Science,* 25 (10), 2008, 1407-1422.
43. Yao, W., Zhang, J., Nadjai, A., Beji, T., and Delichatsios, M. "Development and Validation of a Global Soot Model in Turbulent Jet Flames", *Combustion Science and Technology,* 184 (5), 2012, 717-733.
44. Wang, M., Huang, J., and Bushe, W. K. "Simulation of a turbulent non-premixed flame using conditional source-term estimation with trajectory generated low-dimensional manifold", *Proceedings of the Combustion Institute,* 31 (2), 2007, 1701-1709.
45. Bushea, W. K., and Steiner, H. "Conditional moment closure for large eddy simulation of nonpremixed turbulent reacting flow", *Physics of Fluids,* 11 (7), 1999, 1896-1906.
46. Jones, W. P., and Whitelaw, J. H. "Calculation methods for reacting turbulent flows: a review", *Combustion and Flame,* 48, 1982, 1-26.
47. Malcolm W. Chase, J. "NIST-JANAF thermochemical tables (4th Edition)", *Journal of Physical and Chemical Reference Data,* 9, 1998.

48. Sutherland, W. "The viscosity of gases and molecular force", *Philosophical Magazine Series 5*, 36 (223), 1893, 507-531.
49. Wilke, C. R. "A Viscosity Equation for Gas Mixtures", *The Journal of Chemical Physics*, 18 (4), 1950, 517-519.
50. Saksena, M. P., and Saxena, S. C. "Viscosity of multicomponent gas mixtures", *Proceedings of the Sixth Svmposirun on Thermophvsical Properties*. 31, American Society of Mechanical Engineers, 1973, 100-110.
51. Travin, A. K., Shur, M. L., Spalart, P. R., and Strelets, M. K. "Improvement of Delayed Detached-Eddy Simulation for LES with Wall Modelling", *European Conference on Computational Fluid Dynamics*. TU Delft, The Netherlands, 2006.
52. Shur, M. L., Spalart, P. R., Strelets, M. K., and Travin, A. K. "A Hybrid RANS-LES Approach with Delayed-DES and Wall-Modelled LES Capabilities", *International Journal of Heat and Fluid Flow*, 29, 2008, 1638-1649.
53. Yao, W., Li, X., Wu, K., and Fan, X. "Detached Eddy Simulation of an axisymmetric scramjet combustor fueled by Daqing RP-3 aviation kerosene", *The 8th National Conference on Hypersonic Science and Technology*. Haerbing, 2015, CSTAM2015-A35-B0136.
54. Yao, W., Wang, J., Lu, Y., Li, X., and Fan, X. "Full-scale Detached Eddy Simulation of kerosene fueled scramjet combustor based on skeletal mechanism", *20th AIAA International Space Planes and Hypersonic Systems and Technologies Conference*. Glasgow, Scotland, 2015, AIAA 2015-3579.
55. Yao, W., Wang, J., Lu, Y., and Fan, X. " Skeletal mechanism generation based on DRGEPSA for Daqing RP-3 aviation kerosene and numerical validation", *The 7th National Conference on Hypersonic Science and Technology*. Huairou, Beijing, 2014, CSTAM2014-A62-B0044.
56. Dagaut, P., Karsenty, F., Dayma, G., Di évart, P., Hadj-Ali, K., Mz é-Ahmed, A., Braun-Unkhoff, M., Herzler, J., Kathrotia, T., Kick, T., Naumann, C., Riedel, U., and Thomas, L. "Experimental and detailed kinetic model for the oxidation of a Gas to Liquid (GtL) jet fuel", *Combustion and Flame*, 161 (3), 2014, 835-847.
57. Yao, W., Wang, J., Fan, E., Li, X., and Fan, X. "IDDES study of the flow and combustion characteristics in a RP-3 fueled round-to-elliptical shape-transition supersonic combustor", *The 9th National Conference on Hypersonic Science and Technology*. Xi'an, China, 2016.
58. Niemeyer, K. E., Sung, C.-J., and Raju, M. P. "Skeletal mechanism generation for surrogate fuels using directed relation graph with error propagation and sensitivity analysis", *Combustion and Flame*, 157 (9), 2010, 1760-1770.
59. OpenCFD Ltd. "OpenFOAM 3.0.1". http://www.openfoam.org/, 2015.
60. Wu, K., Li, X., Yao, W., and Fan, X. "Three-Dimensional Numerical Study of the Acoustic Properties of a Highly Underexpanded Jet", *20th AIAA International Space Planes and Hypersonic Systems and Technologies Conference*. AIAA 2015-3572, Glasgow, Scotland, 2015.
61. Li, X., Wu, K., Yao, W., and Fan, X. "A Comparative Study of Highly Underexpanded Nitrogen and Hydrogen Jets Using Large Eddy Simulation", *20th AIAA International Space Planes and Hypersonic Systems and Technologies Conference*. AIAA 2015-3573, Glasgow, Scotland, 2015.
62. Greenshields, C. J., Weller, H. G., Gasparini, L., and Reese, J. M. "Implementation of semi-discrete, non-staggered central schemes in a colocated, polyhedral, finite volume framework, for high-speed viscous flows", *International Journal for Numerical Methods in Fluids*, 38 (2), 2009, 139-161.
63. Li, X., Yao, W., and Fan, X. "Large-Eddy Simulation of Time Evolution and Instability of Highly Underexpanded Sonic Jets", *AIAA Journal*, 54 (10), 2016, 3191-3211.

64. Hirsch, C. *Numerical computation of internal and external flow*. Chichester, U.K.: John Wiley & Sons, 1990.
65. Jasak, H., Weller, H. G., and Gosman, A. D. "High resolution NVD differencing scheme for arbitrarily unstructured meshes", *International Journal for Numerical Methods in Fluids*, 31, 1999, 431-449.
66. Babinsky, H., and Harvey, J. K. *Shock wave-boundary-layer itneractions*. New York: Cambridge University Press, 2011.